Impact of Hovering Inaccuracy on UAV-aided RFET

Suraj Suman, Sidharth Kumar, and Swades De

***Abstract*—In this letter, the impact of hovering inaccuracy on the performance of unmanned aerial vehicle (UAV)-aided RF energy transfer (RFET) is investigated. Hovering inaccuracy is measured by localization and orientation mismatch of UAV while it hovers above a sensor of interest. An analytical framework is presented that captures these mismatches, and its impact on the performance of UAV-aided RFET is studied. To evaluate the performance, a metric called *mismatch index* is defined as the ratio of loss in harvested power due to mismatch and harvested power without mismatch. A closed-form expression of the distribution of mismatch index is obtained. A UAV-based experimental setup is developed to collect the data of hovering inaccuracy parameters, and the performance is investigated for three antenna types with different radiation patterns. It is observed that, the optimal deployment height of UAV increases as the antenna becomes more directional.**

***Index Terms*—Unmanned aerial vehicle (UAV), RF energy transfer, wireless sensor network**

I. Introduction

Now a days, every phenomena related to human, industry, environment, and logistics is connected to the Internet through Internet of Things (IoT) devices, like sensors, actuators, meters, or trackers. The 5G network has to cater to these massive deployment of IoT devices having billions of connections [1]. Limited battery life of these devices is a major hurdle towards automation, as these devices consume significant amount of energy during sensing, processing, and communication [2]. Periodic battery replacement is not an effective solution, because it is costly and not feasible in several applications wherein the devices are deployed at arduous locations. On the other hand, ambient energy sources, such as vibration, ambient RF, piezoelectric, and solar may not ensure perpetual operation due to randomness and unreliability of these sources [3], [4]. Therefore, on-demand wireless energy transfer from dedicated energy source is preferred, and UAV is a perfect choice for this due to its various advantages, namely, excellent maneuverability, autonomous flight, and weight carrying capability.

Sensor nodes control the entire physical phenomena around us, such as, surveillance and monitoring in remote locations, smart farming, and smart warehouse. Online energy replenishment to these nodes is of high importance in order to ensure their perpetual operation. In such sensing applications, UAV-aided RFET is a very good option of powering the sensor nodes, because of the three dimensional mobility of UAV.

This work was supported in part by the Department of Science and Technology—International Bilateral Cooperation Division, under Grant INT/UK/P-153/2017, and in part by the Department of Telecommunications under Grant 4-23/5G test bed/2017-NT for building end-to-end 5G test-bed, along with the Department of Electronics and Information Technology under Visvesvaraya Ph.D. Fellowship Scheme.

The authors are with the Department of Electrical Engineering, Bharti School of Telecom, IIT Delhi, New Delhi 110016, India (e-mail: {suraj.suman, sidharth.kumar, swadesd}@ee.iitd.ac.in).

1) Related work and motivation: There have been a few reported studies in the recent literature, where dedicated UAV-aided wireless energy transfer approaches have been proposed. Magnetic resonance coupling (MRC) based wireless energy transfer using UAV was investigated in [5]. However, MRC performance degrades severely due to vibration, misalignment of coils, and deformation in coils. Moreover, MRC works over very short range, and requires big coils to be mounted on both transmitter and receiver ends, which is not feasible for small sensor nodes deployed at different locations. As a competitive alternative, UAV-based RFET has been reported in [6]–[9]. The authors in [6] proposed strategies for maximizing the received energy at the field sensor nodes, whereas the study in [7] considered the use of the harvested RF energy to maximize information transmission throughput. In [8], charging mechanism was designed to replenish energy reserve of the field sensor nodes using UAV-assisted RFET. The work in [9] presented a wireless charging platform integrated with a quadcopter for large-scale sensing applications.

The works in [6]–[9] do not consider UAV hovering inaccuracy in analysis. Hovering inaccuracy of UAV refers to the error during its execution of mission due to imperfect hovering. Its impact is not severe in UAV-aided cellular architecture due to lesser sensitivity for information transfer and higher operational altitude [10]. In contrast, energy transfer process is quite sensitive to the received energy level, and it operates at much shorter distance [11]. Therefore, accounting of hovering inaccuracy is important for UAV-aided RFET process.

2) Contributions: The key contributions of this work are as follows: (1) An analytical framework for capturing UAV hovering inaccuracy is presented, which comprises of location and orientation mismatches due to positioning error and rotation of UAV, respectively. (2) Variation of distance and elevation angle of the UAV to the ground-deployed node in presence of hovering inaccuracy is analytically characterized using the data collected from a UAV-based experimental setup. (3) A metric, called *mismatch index* is defined for performance evaluation, and a closed-form expression of the distribution of mismatch index is derived. (4) The optimal UAV deployment height is estimated by solving an optimization problem, which maximizes the harvested power for a given hovering inaccuracy.

II. Analysis of hovering inaccuracy

1) System Model: The system model for UAV-aided RFET is shown in Fig. 1, where the RF transmitter mounted on UAV charges the field deployed sensor nodes. Due to poor energy harvesting sensitivity (about -12 dBm) and the associated short feasible RFET range, UAV hovers above each ground-deployed sensor nodes and charges them wirelessly one by one. Energy harvester is embedded in the ground receiver

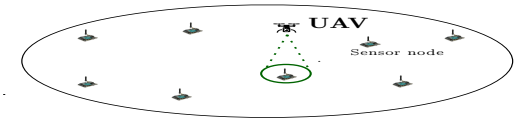

Figure 1: System model for UAV-aided RFET.

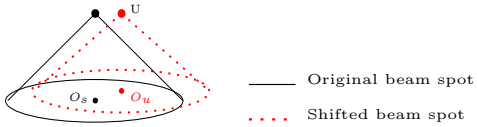

Figure 2: The depiction of localization mismatch.

sensor node, which receives RF power from the UAV-mounted transmitter and converts the radio waves into direct current (DC) power [12]. This DC power is stored in the storage element (supercapacitor) of sensor node for further use.

It is notable here that, the analysis of UAV hovering inaccuracy has considered for single node charging scenario. However, analysis remains valid in a generalized scenario with multiple field node deployment, because other nodes will also experience UAV hovering inaccuracy during their RFET turn.

The location of sensor node that is to be charged and the hovering altitude are fetched in UAV from ground control station (GCS). The GCS-controlled UAV arrives at a given sensor's location and facilitates UAV-assisted RFET. While facilitating UAV-aided RFET, it is desired that, UAV hovers just above a given sensor node at given altitude and remains stationary while charging the sensor node, which ensures maximum energy transfer. However, this does not happen due to positioning error from global positioning system (GPS)-termed as localization mismatch (LM), and angular displacement that arises from rotation of UAV-termed as orientation mismatch (OM). These two mismatches are analyzed here.

2) Effect of localization mismatch:: Let L_o^s and L_a^s be respectively the longitude and latitude of sensor node positioned at O_s (see Fig. 2) above which UAV is supposed to hover at an altitude. Instead, due to positioning inaccuracy, UAV hovers above O_u, with longitude and latitude L_o^u and L_a^u. The transformation from longitude and latitude to Cartesian coordinate is obtained as follows [13]:

$$x_s = R_e \cdot \cos(L_a^s) \cdot \cos(L_o^s),\ x_u = R_e \cdot \cos(L_a^u) \cdot \cos(L_o^u)$$
$$y_s = R_e \cdot \cos(L_a^s) \cdot \sin(L_o^s),\ y_u = R_e \cdot \cos(L_a^u) \cdot \sin(L_o^u)$$

where x_s and y_s are the Cartesian coordinates of the sensor node located at O_s; x_u and y_u are the co-ordinates of the location on O_u; $R_e = 6378136.047$ m is the radius of earth.

This localization mismatch has significant impact on the system layout, which alters the separation and elevation angle between sensor node and RF transmitter. The distance d between a UAV-mounted transmitter and the sensor node's RF energy receiver due to this error is expressed as:

$$d = \sqrt{(x_s - x_u)^2 + (y_s - y_u)^2 + h^2}. \quad (1)$$

where h is the hovering altitude of UAV.

The elevation angle Φ_{LM} between sensor node and energy transmitter due to this position error is obtained as:

$$\Phi_{LM} = \arctan\left[\sqrt{(x_s - x_u)^2 + (y_s - y_u)^2}/h\right]. \quad (2)$$

3) Effect of orientation mismatch: UAV has translational and rotational degrees of freedom [14]. However, a hovering UAV undergoes only rotational motion. There are three types of rotational motion: *pitch, roll*, and *yaw* as depicted in Fig. 3(a). *Pitch* corresponds to rotation around the lateral axis or around the wings, *roll* corresponds to rotation around the longitudinal axis or around the head, whereas *yaw* corresponds to rotation around the vertical plane. Let *pitch, roll*, and *yaw* correspond to x, y, and z-axis, respectively, for analysis.

The center of beam spot of the transmitter antenna mounted on UAV is displaced due to the rotation, and the antenna's beam does not point towards the receiver antenna. The displacement due to *roll* and *pitch* are illustrated respectively in Fig. 3(b) and Fig. 3(c). Due to these rotations, the center of beam spot is displaced about the corresponding axes, but the transmitter-receiver distance does not change. The rotation along *pitch* and *roll* lead to shift of beam spot respectively along the x-axis and y-axis. Fig. 3(e) depicts the shift of center of beam spot along *roll*. If UAV hovers at altitude h, then the displacement in center of beam spot due to rotation of angle θ_R along *roll* and angle θ_P along *pitch* are expressed as:

$$\tan\theta_R = \frac{y_r}{h} \Rightarrow y_r = h \cdot \tan\theta_R;\ \ x_r = h \cdot \tan\theta_P, \quad (3)$$

x_r and y_r denote the shift in center of beam spot due to rotation along *roll* and *pitch*, respectively, with $\theta_P, \theta_R \in [-\frac{\pi}{2}, \frac{\pi}{2}]$.

The rotational motion does not change the distance between sensor node and transmitter, but the orientation of transmitter antenna with respect to receiver antenna changes. The elevation angle Φ_{OM} between the sensor node's antenna and transmitter due to orientation mismatch is expressed as:

$$\Phi_{OM} = \arctan\left[\sqrt{x_r^2 + y_r^2}/h\right]. \quad (4)$$

The rotation along *yaw* does not change the separation between transceiver and the elevation angle Φ_{OM}, as it rotates the beam only and does not change the center of beam spot (see Fig. 3(d)). However, the azimuth angle on ground plane will change due to *yaw*, which can be overcome by using transmitter antenna having symmetric radiation pattern in azimuth plane [15]. The change in polarization of incident wave is the other problem arises due to rotation, which can be mitigated by using the rectenna with polarization diversity capability to avoid the polarization mismatches and losses caused by unknown or time-varying polarization of incident electromagnetic waves [16]. Since, the appropriate antenna pattern can fairly mitigate the effect of *yaw*, performance degradation analysis in this work does not account for *yaw*.

III. Effects of Mismatch on System Layout

The discussions Section II reveal that, UAV hovers at slightly different location due to positioning error, and at this location UAV undergoes rotational motion rather than being stationary. Localization mismatch lead to change in distance and elevation angle between transmitter-receiver, whereas orientation mismatch leads to change in elevation angle. By including the effect of both mismatches, it is deduced that the distance between transmitter and receiver is same as in (1), whereas elevation angle is different from those expressed

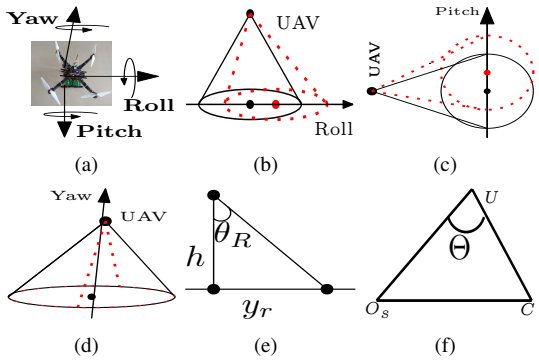

Figure 3: (a) The three rotational axes of UAV; depiction of shift in beam spot due to rotation along (b) roll, (c) pitch, (d) yaw; (e) geometrical representation of displacement of beam spot along roll; (f) depiction of elevation angle between sensor node's receiver antenna and transmitter antenna mounted on UAV.

in (2) and (4), which needs to be evaluated. Let $C(x_c, y_c, 0)$ be shifted center of beam spot due to both mismatches, i.e., localization and orientation mismatch, which is written as:

$$C \equiv (x_c, y_c, 0) \equiv (x_u + x_r, y_u + y_r, 0). \tag{5}$$

The coordinates of three points O_s, U, and C are obtained. Thus, referring to Fig. 3(f), the elevation angle Θ between the shifted beam center C and the sensor node placed at O_s with the UAV antenna located at U is given as:

$$\Theta = \arccos\left[(\overrightarrow{UO_s} \cdot \overrightarrow{UC})/(|\overrightarrow{UO_s}| \cdot |\overrightarrow{UC}|)\right] \tag{6}$$

where $\overrightarrow{UO_s} = [x_s - x_u, y_s - y_u, -h]$ and $\overrightarrow{UC} = [x_c - x_u, y_c - y_u, -h]$. $\overrightarrow{UO_s} \cdot \overrightarrow{UC}$ denotes the dot product of $\overrightarrow{UO_s}$ and $\overrightarrow{UC}$.

Form the geometrical illustration and analysis presented above, it can be deduced that $\Phi_{LM} - \Phi_{OM} \leq \Theta \leq \Phi_{LM} + \Phi_{OM}$. The boundary cases lead to the condition when O_s, O_u, and C are collinear. If C is towards O_s then $\Theta = \Phi_{LM} - \Phi_{OM}$, whereas if C is away from O_s then $\Theta = \Phi_{LM} + \Phi_{OM}$.

IV. Impact of Hovering Inaccuracy

With the positional and rotational inaccuracy characterization above, in this section we compute the impact of hovering inaccuracy in terms of reduced amount of harvested power. The power received at a sensor node is obtained as: $P_r = P_t \cdot G_r \cdot g(\varphi) \cdot (\lambda/4\pi d_{tr})^2$, where P_t is the power transmitted by transmitter mounted on UAV, $g(\varphi)$ is the radiation pattern of transmitter antenna having elevation angle φ between transmitter and receiver, G_r is the receiver antenna gain, d_{tr} is the distance between transmitter and receiver, and λ is the wavelength of operational RF wave. The received power at the sensor node depends on distance and elevation angle between transceiver. Therefore, the harvested power at sensor nodes also differ significantly.

The received power at sensor node without localization and orientation mismatch, when UAV hovers at altitude h, is expressed as: $P_o(h) = P_r|_{\varphi=0,\, d_{tr}=h}$.

The received power at sensor node in presence of localization and orientation mismatch is: $P_M(h, \varphi) = P_r|_{\varphi=\Theta,\, d_{tr}=d}$, where d_{tr} and Θ are obtained respectively in (1) and (6).

It may be noted that, fading effects are not accounted in the hovering inaccuracy analysis. Large-scale fading has no effect on the system design, because UAV hovers just above the sensor node, and distance between UAV-mounted transmitter and receiver field node is quite short [17]. On the other hand, small-scale fading is averaged out due to longer time scale of RFET on the order of several minutes [18].

It can be noted that, the received power differs significantly in presence of mismatches. This will also alter the harvested power. An important question to ask while assessing the UAV-assisted RFET performance is, *the reduction of harvested power in presence of mismatches as compared to the desired harvested power without mismatches*.

For this purpose, a metric called *mismatch index* $\mathcal{M}$ is defined, which is the ratio of loss in harvested power due to mismatch and the estimated harvested power without mismatch. $\mathcal{M}$ ($0 \leq \mathcal{M} \leq 1$) indicates the deviation from the ideal case, for different system design parameters, i.e., deployment altitude and antenna pattern. Thus, $\mathcal{M}$ is given as:

$$\mathcal{M}(h) = 1 - \frac{P_{\mathcal{H}}(P_M(h, \varphi = \Theta))}{P_{\mathcal{H}}(P_o(h))} \tag{7}$$

where $P_{\mathcal{H}}(\cdot)$ denotes the harvested power, which has been empirically obtained through the curve-fitting as [19]: $P_{\mathcal{H}}(p) = \frac{\mathsf{T}}{1-\Omega}\left[\frac{1}{1+\exp[-\alpha(p-\beta)]} - \Omega\right]$ with received power p, $\mathsf{T} = 24$ mW, $\alpha = 150$, $\beta = 0.0014$, $\Omega = 1/[1 + \exp(\alpha \cdot \beta)]$.

Mismatch index is a reasonable metric for multiple sensor charging scenario, because other nodes will also be affected by the hovering inaccuracy during their RFET process.

V. Results and Discussions

Rotatory-wing UAV can hover at a particular altitude for several minutes, therefore it is preferred over fixed-wing UAV. A customized rotatory-wing UAV (cf. Fig. 4(a)) has been assembled to conduct experiments and collect relevant data.

1) Experimental setup: The experimental setup is shown in Fig. 4(a), where an electronic device as representative load equivalent to transmitter is attached at the bottom of UAV. The GPS location of the sensor node placed at ground and altitude of operation are fed into the Ardupilot mission planner (http:ardupilot.org), which is installed in the computer acting as GCS. The UAV setup (see Fig. 4(a)) hovers at different altitude from 1 m to 5 m, for approximately three minutes at each altitude. The data of GPS location and rotational motion parameter of UAV are collected for analysis.

2) Variation of different parameters: The parameter values are studied and fitted using curve fitting technique for ease of analysis. The fitted equations along with the fitting coefficients are listed in Table I. The R-square values for fitting equations are listed, and its value close to 1 indicates the best fit.

The GPS location of a known reference point is fed into UAV. The GPS location of UAV when it hovers at different altitude is collected. Then, the distance, and elevation angle between UAV-mounted transmitter and receiver on ground are calculated from respectively (1) and (2), and noted in Table I.

The variation of elevation angle due to orientation mismatch is obtained from (4). It is observed that, Φ_{OM} closely follows Gaussian shape for data set of each height, i.e., 1 to 5 m, and is

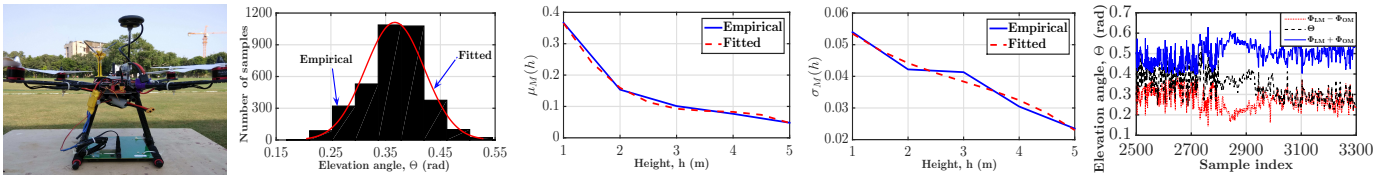

(a) Experimental set up (b) histogram of Θ at $h = 1$ m (c) mean of Θ (d) standard deviation of Θ (e) bounds on Θ

Figure 4: UAV experimental setup; performance results, and their analyses.

$$
\begin{aligned}
p_1 &= \big[\psi(\lambda(p)) - \mu(h)\big]/\sigma(h), p_2 = \big[-\psi(\lambda(m)) - \mu(h)\big]/\sigma(h), p_3 = \big[\sqrt{\psi(\lambda(m))} - \mu(h)\big]/\sigma(h),\\
p_4 &= \big[-\sqrt{\psi(\lambda(m))} - \mu(h)\big]/\sigma(h), p_5 = \big[\sqrt{\psi(-\lambda(m))} - \mu(h)\big]/\sigma(h), p_6 = \big[-\sqrt{\psi(-\lambda(m))} - \mu(h)\big]/\sigma(h).\\
m_1 &= \big[\psi(\nu(m)) - \mu(h)\big]/\sigma(h), m_2 = \big[-\psi(\nu(m)) - \mu(h)\big]/\sigma(h), m_3 = \big[\sqrt{\psi(\nu(m))} - \mu(h)\big]/\sigma(h),\\
m_4 &= \big[-\sqrt{\psi(\nu(m))} - \mu(h)\big]/\sigma(h), m_5 = \big[\sqrt{\psi(-\nu(m))} - \mu(h)\big]/\sigma(h), m_6 = \big[-\sqrt{\psi(-\nu(m))} - \mu(h)\big]/\sigma(h).
\end{aligned} \tag{8}
$$

Table I: Variation of different parameters.

Localization Mismatch	$d(h) = \sqrt{u_1 h^2 + u_2 h + u_3}$; R-square $= 0.9999$ $u_1 = 1.015, u_2 = -0.1193, u_3 = 0.2588$, $\Phi_{LM}(h) = v_1 h^3 + v_2 h^2 + v_3 h + v_4$; R-square $= 0.9938$ v_1=−0.01573, v_2=0.1763, v_3=−0.651, v_4=0.8488.
Orientation Mismatch	$\Phi_{OM} \sim \mathcal{N}\big(\mu_{OM}(h), \sigma^2_{OM}(h)\big)$, $\mu_{OM}(h) = w_1 h^3 + w_2 h^2 + w_3 h + w_4$; R-square=0.9976 w_1=0.00125, w_2=−0.01073, w_3=0.01871, w_4= 0.0623, $\sigma_{OM}(h) = z_1 h^3 + z_2 h^2 + z_3 h + z_4$; R-square $= 0.9819$ z_1=−0.001128, z_2=0.009966, z_3=−0.03044, z_4=0.06542.
Both Mismatch	$\Theta \sim \mathcal{N}\big(\mu_M(h), \sigma^2_M(h)\big)$, $\mu_M(h) = a_1 h^3 + a_2 h^2 + a_3 h + a_4$; R-square $= 0.9977$ a_1=−0.01371, a_2=0.1518, a_3=−0.5653, a_4=0.7925, $\sigma_M(h) = b_1 h^3 + b_2 h^2 + b_3 h + b_4$; R-square $= 0.9686$ b_1=−0.000584,b_2=0.00523,b_3=−0.0209, b_4 =0.06973.

modeled as: $\Phi_{OM} \sim \mathcal{N}\big(\mu_{OM}(h), \sigma_{OM}(h)\big)$, where $\mu_{OM}(h)$ and $\sigma_{OM}(h)$ respectively denote the mean and standard deviation at height h, and are presented in Table I.

The variation of elevation angle arises due to localization and orientation mismatch (Θ, given in (6)), and its histogram is shown in Fig. 4(b) for $h = 1$ m. Significant variation in Θ is observed and its distribution closely follows Gaussian shape. It is noticed that, the distribution of Θ for other heights also follow Gaussian distribution. Therefore, the elevation angle Θ is found to vary with Gaussian distribution as: $\Theta \sim \mathcal{N}\big(\mu_M(h), \sigma_M(h)\big)$, where $\mu_M(h)$ and $\sigma_M(h)$ respectively denote the mean and standard deviation at height h, and expressed in Table I. The variation of original and fitted values of mean and variance are shown in respectively Fig. 4(c) and Fig. 4(d). Fig. 4(e) verifies the bound of Θ, i.e., $\Phi_{LM} - \Phi_{OM} \leq \Theta \leq \Phi_{LM} + \Phi_{OM}$.

The effect of hovering inaccuracy reduces with increase in hovering altitude of UAV. This can be interpreted as follows: Localization mismatch reduces with increase in altitude, because shift in the center of beam spot does not increase in the same proportion with altitude. On the other hand, orientation mismatch also reduces with altitude, because the air reverts back and collides with UAV at low altitude operation, which makes it vibrate a little bit more compared to that at higher altitude. The pushed down air has more space to dissipate at higher hovering altitude, and hence stability increases due to less turbulence. To verify this fact mathematically, it requires to investigate the nature of mean and standard deviation of Θ. The first derivative of mean and standard deviation of Θ are obtained as: $\frac{d}{dh}\mu_M(h) = 3a_1h^2 + 2a_2h + a_3$, $\frac{d}{dh}\sigma_M(h) = 3b_1h^2 + 2b_2h + b_3$. $\frac{d}{dh}\mu_M(h) < 0$ because the discriminant of $\frac{d}{dh}\mu_M(h)$, i.e., $\Delta_{\mu_M} = 4[a_2^2 - 3a_1a_3] < 0$ and $a_1 < 0$. Likewise, $\frac{d}{dh}\sigma_M(h) < 0$, because the discriminant of $\frac{d}{dh}\sigma_M(h)$, i.e., $\Delta_{\sigma_M} = 4[b_2^2 - 3b_1b_3] < 0$ and $b_1 < 0$. This analysis also verifies decreasing nature of elevation angle with altitude.

3) Performance analysis: Three different types of antenna having different beam width (BW) are considered as follows:

$$
g(\varphi) = \begin{cases} D_1, & \text{A}_1, \quad \text{Isotropic} \\ D_2 \cdot \cos(\varphi), & \text{A}_2, \quad \text{BW} = \frac{2\pi}{3} \\ D_3 \cdot \cos^2(\varphi), & \text{A}_3, \quad \text{BW} = \frac{\pi}{2} \end{cases},
$$

where $D_1 = 1, D_2 = 4, D_3 = 6$ [15]. The values of other parameters are: $P_t = 3$ W, $G_r = 2.1$, $f = 0.915$ GHz.

The cumulative distribution function (CDF) $F_{P_{r(h)}}(p)$ of received power when UAV hovers at altitude h, is given by,

$$
F_{P_{r(h)}}(p) = \begin{cases} \mathcal{U}(p - \rho), & \text{A}_1 \\ 1 + \text{Q}(p_1) - \text{Q}(p_2), & \text{A}_2 \\ \text{Q}(p_3) - \text{Q}(p_4) - \text{Q}(p_5) + \text{Q}(p_6), & \text{A}_3 \end{cases}
$$

where $\mathcal{U}(\cdot)$ denotes the unit step function. $\rho = P_t G_r D_1 (\lambda/4\pi d_{tr})^2$. $\text{Q}(\cdot)$ denotes the Q-function. The expression for $p_i, i = 1, \cdots, 6$ are given in (8) $\psi(\lambda(\cdot)) = \arccos(\lambda(\cdot))$, $\lambda(p) = (pd^2)/(h^2 P_o(h))$.

The CDF of received power, $F_{P_{r(h)}}(p)$, for different antenna with deployment altitude of 1 m is shown in Fig. 5. The CDF is deterministic for antenna A_1 due to its isotropic nature, which overcomes the randomness caused by orientation mismatch; randomness arises only due to localization mismatch. Randomness in received power is more severe for antenna 3. This is because, a wider beam width overcomes the effect of randomness more easily. One can observe that, the received power in presence of hovering inaccuracy is lesser than the estimate ideal case, i.e., in absence of mismatches. A few dB deviation in received power has significant impact on the system performance; ignoring this deviation may lead to under-dimensioning of UAV-aided RFET system design. $F_{P_{r(h)}}(p)$ obtained from analysis closely matches with that obtained from empirical data collected from UAV experimental setup, which validates correctness of the closed-form expression.

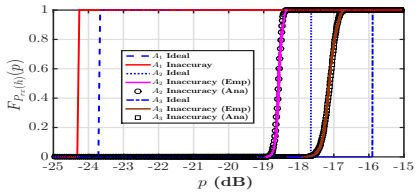

Figure 5: CDF of received power for different antenna with height $h = 1$ m; Emp: empirical, Ana: Analytical.

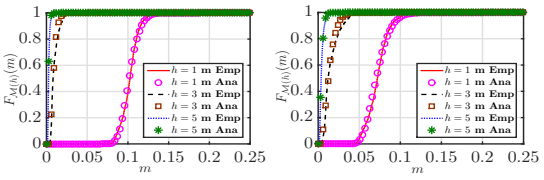

(a) A_2 (b) A_3

Figure 6: CDF of *mismatch index* for different height and antenna.

The cumulative distribution function (CDF) of *mismatch index* $F_{\mathcal{M}(h)}(m)$, when UAV hovers at altitude h, is obtained from (7) using the distribution of Θ (see Table I) through transformation of random variable. $F_{\mathcal{M}(h)}(m)$ is given by:

$$F_{\mathcal{M}(h)}(m) = \begin{cases} \mathcal{U}(m-\varrho), & \text{A}_1 \\ -\text{Q}(m_1) + \text{Q}(m_2), & \text{A}_2 \\ 1 - \text{Q}(m_3) + \text{Q}(m_4) + \text{Q}(m_5) - \text{Q}(m_6), & \text{A}_3 \end{cases}$$

$\varrho = 1 - \left(\frac{1}{1+\exp[-\alpha(P_M(h,\varphi)-\beta)]} - \Omega\right) / \left(\frac{1}{1+\exp[-\alpha(P_o(h)-\beta)]} - \Omega\right)$ with $K_0 = \left[\frac{1}{1+\exp[-\alpha(P_o(h)-\beta)]} - \Omega\right]$. The expressions of $m_i \quad i = 1, \cdots, 6$ are given in (8) with $\nu(m) = \frac{d^2}{h^2 P_o(h)}\left[\beta - \frac{1}{\alpha}\left(\ln\left(-1 + \frac{1}{\Omega + (1-m)K_0}\right)\right)\right]$.

The CDF $F_{\mathcal{M}(h)}(m)$, is deterministic for antenna A_1, because isotropic nature of A_1 due to its isotropic nature. The value of $\varrho = 0.1157, 0.0234, 0.0041$ for $h = 1, 3, 5$ m, respectively. The variation of $F_{\mathcal{M}(h)}(m)$ for antennas A_2 and A_3 for different height are shown in Fig. 6. The close match of $F_{\mathcal{M}(h)}(m)$ obtained from analysis and empirical data collected from UAV experimental setup validates correctness of the closed-form expression. It can be observed that, the hovering inaccuracy affects significantly the harvested power at sensor node due to reduction in received power (cf. Fig. 5), and the effect of mismatch reduces with increased height, as mean and standard deviation of Θ decrease with height.

4) Optimal hovering altitude estimation: We observed that, the sensor node receives different power level and hence different amount of harvested power due to hovering inaccuracy. It is important to eliminate the deployment altitude where the harvested power is maximum and the estimation error due to inaccuracy should lie in a tolerable range. This condition is useful in several applications, such as in harvest and transmit protocol, where energy is harvested first before transmitting data. The optimization problem for obtaining the optimal altitude is formulated as follows:

$$\max_h \mathbb{E}[P_{\mathcal{H}}(P_M(h, \varphi = \Theta))] = \mathbb{E}[(1 - \mathcal{M}(h))P_o(h, \varphi)]$$

$$\text{s. t. : (C1)} : F_{\mathcal{M}(h)}(m_{th}) \geq \kappa; \ \text{(C2)} : h_{min} \leq h \leq h_{max}.$$

Constraint (C1) restricts the mismatch up to m_{th} to ensure the power availability at sensor node, whereas constraint (C2) indicates the range of hovering altitude of UAV. It is deduced from the analysis presented in previous subsection that, constraint (C1) is not a convex function. Therefore, this optimization problem is not a convex function, and hence *golden-section method* is used to solve it numerically [20]. The optimal height is 1.13 m, 1.35 m, and 1.47 m, respectively for antenna A_1, A_2, and A_3 with $m_{th} = 0.1, \kappa = 0.9$.

VI. Concluding Remarks

In this work, hovering inaccuracy of UAV-aided RFET performance has been studied. Besides characterization of different mismatch parameters, a term called *mismatch index* has been defined through which RFET performance-degradation is quantified. Analytical characterization and performance have been verified through experimental UAV-hovering data along with the given system parameters. The expressions will be useful in UAV-aided RFET performance optimization.

References

[1] Z. Dawy *et al.*, "Toward massive machine type cellular communications," *IEEE Wireless Commun.*, vol. 24, no. 1, pp. 120–128, Feb. 2017.

[2] B. Martinez *et al.*, "The power of models: Modeling power consumption for IoT devices," *IEEE Sensors J.*, vol. 15, no. 10, pp. 5777–5789, Oct. 2015.

[3] A. Costanzo and D. Masotti, "Energizing 5G: Near- and far-field wireless energy and data trantransfer as an enabling technology for the 5G IoT," *IEEE Microw. Mag.*, vol. 18, no. 3, pp. 125–136, May 2017.

[4] S. Suman and S. De, "Solar-enabled green base stations: Cost versus utility," in *Proc. IEEE WoWMoM*, Macau, China, June 2017, pp. 1–8.

[5] B. Griffin and C. Detweiler, "Resonant wireless power transfer to ground sensors from a UAV," in *Proc. IEEE Int. Conf. Robot. Autom.*, Saint Paul, MN, USA, May 2012, pp. 2660–2665.

[6] J. Xu *et al.*, "UAV-enabled wireless power transfer: Trajectory design and energy optimization," *IEEE Trans. Wireless Commun.*, vol. 17, no. 8, pp. 5092–5106, Aug. 2018.

[7] L. Xie *et al.*, "Throughput maximization for UAV-enabled wireless powered communication networks," *IEEE Internet of Things J.*, vol. 6, no. 2, pp. 1690–1703, Apr. 2019.

[8] S. Suman *et al.*, "UAV-assisted RF energy transfer," in *Proc. IEEE Int. Conf. Commun.*, Kansas City, MO, USA, May 2018, pp. 1–6.

[9] J. Chen *et al.*, "Q-charge: A quadcopter-based wireless charging platform for large-scale sensing applications," *IEEE Netw.*, vol. 31, no. 6, pp. 56–61, Nov. 2017.

[10] S. Kumar *et al.*, "Backhaul and delay-aware placement of UAV-enabled base station," in *Proc. IEEE INFOCOM Wksp.*, Honolulu, HI, USA, Apr. 2018, pp. 634–639.

[11] S. De *et al.*, "On the feasibility of network RF energy operated field sensors," in *IEEE Int. Conf. Commun.*, Cape Town, South Africa, May 2010, pp. 1–5.

[12] Powercast. [Online]. Available: http://www.powercastco.com.

[13] C. T. Russell, "Geophysical coordinate transformations," *Cosmic Electrodynamics*, vol. 2, no. 2, pp. 184–196, 1971.

[14] J. D. Barton, "Fundamentals of small unmanned aircraft flight," *Johns Hopkins APL technical digest*, vol. 31, no. 2, pp. 132–149, 2012.

[15] C. A. Balanis, *Antenna Theory: Analysis and Design*. John Wiley & Sons, Inc, 2005.

[16] H. Sun and W. Geyi, "A new rectenna with all-polarization-receiving capability for wireless power transmission," *IEEE Antennas Wireless Propag. Lett*, vol. 15, pp. 814–817, Sep. 2016.

[17] S. Suman *et al.*, "Path loss model for UAV-assisted RFET," *IEEE Commun. Lett.*, vol. 22, no. 10, pp. 2048–2051, Oct. 2018.

[18] ——, "UAV-assisted RFET: A novel framework for sustainable WSN," *IEEE Trans. Green Commun. Netw.*, to be published, doi: 10.1109/TGCN.2019.2938403.

[19] E. Boshkovska *et al.*, "Practical non-linear energy harvesting model and resource allocation for SWIPT systems," *IEEE Commun. Lett.*, vol. 19, no. 12, pp. 2082–2085, Dec. 2015.

[20] D. P. Bertsekas, *Nonlinear programming*. Athena Scientific Belmont, 1999.